Scripta Materialia 210 (2022) 114450

Contents lists available at ScienceDirect

Scripta Materialia

journal homepage: www.elsevier.com/locate/scriptamat

Short-range order localizing diffusion in multi-principal element alloys

Bin Xing[a], Xinyi Wang[b,c], William J. Bowman[a,d], Penghui Cao[b,a,c,*]

[a] Department of Materials Science and Engineering, University of California, Irvine, CA 92697, United States
[b] Department of Mechanical and Aerospace Engineering, University of California, Irvine, CA 92697, United States
[c] Materials and Manufacturing Technology Program, University of California, Irvine, CA 92697, United States
[d] Irvine Materials Research Institute, University of California, Irvine, CA 92697, United States

ARTICLE INFO

Article history:
Received 25 August 2021
Revised 22 November 2021
Accepted 26 November 2021

Keywords:
High-entropy alloy
Short-range order
Local chemical order
Diffusion correlation
Energy barrier

ABSTRACT

The impact of chemical short-range order (SRO) on diffusion is computationally studied and theoretically analyzed in two classes of multi-principal elements alloys, *fcc* CrCoNi and *bcc* MoNbTa. We find the presence of SRO considerably reduces and localizes vacancy-mediated diffusion. The diffusivity reduction is induced by an increase of migration barrier (decreasing jump frequency) and enhanced diffusion correlation that lowers the effectiveness of atomic jumps. By sampling the diffusion pathways and associated energy barriers, a picture of SRO-stretched potential energy landscape is conceived that elucidates an increasing backward jumps and vacancy trapping effect stemming from chemical ordering. The results imply controlling the ordering in chemistry can act as a potential approach for manipulating diffusional behaviors in multi-principal elements alloys.

© 2021 Acta Materialia Inc. Published by Elsevier Ltd. All rights reserved.

Diffusion involving matter transport from one point to another is essential to the fundamental understanding of many kinetic processes such as annealing, precipitation, and creep at elevated temperatures [1]. The multi-principal element alloys, commonly known as high-entropy alloys (HEAs) [2,3] consisting of multiple principal elements in high concentration, receive growing attention due to their extraordinary properties, including high thermal stability [4], high-temperature strength and creep resistance[5], enhanced radiation tolerance [6], and good corrosion resistance [7]. Most of these properties and behaviors are closely related to or mainly governed by diffusion kinetics. One of the salient features pertaining to HEAs and making them different from traditional dilute alloys is short-range order [8]. The formed local chemical order due to solute-solute interactions considerably impacts mechanical behaviors of HEAs, for example, favored planar slip and improved yielding strength [9]. When short-range order appears, a fundamental question as to its role on diffusion arises and remains to be answered: how does the local chemical order influence atomic jumps and diffusional behavior [10]? Using atomistic modeling and theoretical analysis, we aim to address this question and fundamentally understand the impact of local chemical order on self-diffusion in HEAs.

From a microscopic perspective, diffusion occurs by motion of constituent particles, and the Einstein-Smoluchowski equation [11,12] relates the diffusion coefficient (rate of diffusion or diffusivity) D to the mean square displacement of diffusing particles, $D = < \boldsymbol{R}^2 > /6t$, where $< \boldsymbol{R}^2 >$ represents the mean square displacement of an ensemble of particles over time t. In crystalline solids, atom diffusion occurs by elementary atomic jump on the lattice, for instance, jump of an atom from its lattice site to a neighboring vacant site in the presence of vacancy [1]. The total displacement of a particle after a sequence of n number of jumps can be written as $\boldsymbol{R} = \sum_{i=1}^{n} \boldsymbol{r}_i$, where $\boldsymbol{r}_i$ is the ith jump vector. The squared magnitude of net displacement of the atom is calculated as $\boldsymbol{R}^2 = \sum_{i=1}^{n} \boldsymbol{r}_i{}^2 + 2\sum_{i=1}^{n-1}\sum_{j=i+1}^{n} \boldsymbol{r}_i \boldsymbol{r}_j$. For vacancy-mediated diffusion it becomes $\boldsymbol{R}^2 = n\lambda^2 + 2\lambda^2 \sum_{i=1}^{n-1}\sum_{j=i+1}^{n} \cos\theta_{ij}$, where λ is the jump length equal to the first nearest-neighbor distances, and θ denotes the angle between i and j jumps. Averaging over the ensemble of atoms, one can obtain the mean square displacement (MSD), $< \boldsymbol{R}^2 > = \lambda^2 < n > + 2\lambda^2 \sum_{i=1}^{n-1}\sum_{j=i+1}^{n} < \cos\theta_{ij} >$.

The first term $\lambda^2 < n >$ in the above equation captures the mean square of all individual jump distance, here we call it accumulative mean square displacement (aMSD) for the sake of distinguishing it from MSD, $< \boldsymbol{R}^2 >$. The double sum term, $2\lambda^2 \sum_{i=1}^{n-1}\sum_{j=i+1}^{n} < \cos\theta_{ij} >$, considers the averages between i and j jumps, standing for correlation effect. For purely random and uncorrelated diffusion, each jump direction is independent of all previous jumps, and $\sum_{i=1}^{n-1}\sum_{j=i+1}^{n} < \cos\theta_{ij} >$ becomes zero because on average $\cos\theta_{ij}$ has an equal chance of being negative and positive. The mean square displacement $< \boldsymbol{R}^2 >$ and accumulative mean displacement $\langle \boldsymbol{R}^2{}_a \rangle$ are therefore equivalent and both equal to $\lambda^2 < n >$. Concerning non-random diffusion, the correlation factor f can be expressed as a function of MSD and aMSD,

* Corresponding author.
E-mail address: caoph@uci.edu (P. Cao).

https://doi.org/10.1016/j.scriptamat.2021.114450
1359-6462/© 2021 Acta Materialia Inc. Published by Elsevier Ltd. All rights reserved.

$f = 1 + 2\lambda^2 \sum_{i=1}^{n-1} \sum_{j=i+1}^{n} < \cos\theta_{ij} > /\lambda^2 n = < \boldsymbol{R}^2 > / < \boldsymbol{R}^2{}_a >$. With the microscopic diffusion theory, we perform atomistic simulation and modeling to understand diffusional behavior in MPEAs and reveal the impact of short-range order on it, if any.

We consider two distinct types of model systems, *fcc* CrCoNi and refractory *bcc* NbMoTa alloys with equimolar compositions. The atomic configurations that consist of 256,000 and 128,000 atoms for CrCoNi and NbMoTa, respectively, are constructed by inserting particles with randomly assigned atom types, corresponding to random solid solutions (RSS). We adopt an embedded-atom-method potential [13] for describing interatomic interactions in CrCoNi and a machine learning potential [14] for NbMoTa, and both force fields have been tested for reproducing accurate solute-solute interactions and hence chemical ordering. To enable SRO formation, we use a Monte Carlo (MC) swap of atoms coupled with MD simulations [15]. For CrCoNi alloy, the hybrid MC/MD simulations are carried out under the variance-constrained semi-grand-canonical ensemble. The simulation is run at 650 K for 1 million MD timesteps, in which every 100 steps involve one MC cycle consisting of 512,000 trial moves. The MC/MD simulations of NbMoTa are performed under canonical ensemble at 300 K with Nose-Hoover thermostat [16,17]. The simulation involves 100,000 MD steps and calls MC every 100 timesteps to perform trials of exchanging each pair of elements. It is worth noting that the MC-based method, incapable of modeling the kinetics associated with SRO formation, aims to create lower energy states with SRO formation, which enables us to study SRO effects on atom diffusion barriers and pathways.

Figs. 1a, c show the representative atomic configurations with RSS and SRO for CrCoNi and NbMoTa, respectively. We use the non-proportional number to quantify the degree of chemical order [18]. The order parameter between any pair of atom i and j is defined as $\delta_{ij}^k = N_{ij}^k - N_{0,\ ij}^k$, where N_{ij}^k denotes the actual number of pairs in kth shell, and $N_{0,\ ij}^k$ is the number of pairs for the pure random mixture (its value depending on the atomic ratio and structure type, *fcc* or *bcc*). We can see a positive δ_{ij}^k indicates a favored and increased number of pairs, meaning element i tends to bond with element j in the kth shell, while a negative value represents an unfavored pairing. Fig. 1b shows the calculated order parameters δ_{ij} for the first nearest neighboring shell in CrCoNi. The values of all pairs in our RSS system are zeros, indicating the random nature of our model. The MC/MD annealed structure exhibits favored Ni-Ni and Co-Cr pairs, with parameters 2.86 and 1.90, respectively. Unfavored pairs occur between Ni-Co, Ni-Cr, and Cr-Cr with negative values of −1.9, −0.96, −0.95. The short-range order parameters for NbMoTa alloys are shown in Fig. 1d. Strong ordering happens to the pair between Mo and Ta ($\delta_{\text{Ta-Mo}}^{k=1} = 1.54$), with both Mo and Ta atoms tending to leave the first shell centered by themselves and indicating the self-repulsion interaction. Compared with the other two elements, the ordering of Nb atoms is less notable, with a weak attraction between Nb-Mo and repulsion between Nb-Ta.

The MSD can be directly computed by tracking positions $\boldsymbol{x}$ of all N atoms as a function time t, $< \boldsymbol{R}^2 > (t) = \frac{1}{N} \sum_{i=1}^{N} |\boldsymbol{x}_i(t) - \boldsymbol{x}_i(0)|^2$. The accumulative mean square displacement $\langle \boldsymbol{R}^2{}_a \rangle$ can be measured by summing all the contributions from individual jumps during a time interval δt, as $< \boldsymbol{R}^2{}_a > (t) = \frac{1}{N} \sum_{v=\delta t}^{t} \sum_{i=1}^{N} |\boldsymbol{x}_i(v) - \boldsymbol{x}_i(v - \delta t)|^2$. Therefore, aMSD $< \boldsymbol{R}^2{}_a >$ reflects the actual jump frequency, and the MSD $< \boldsymbol{R}^2 >$ quantifies diffusivity by considering the effectiveness of atomic jumps (i.e., correlation effect). To enable the modeling of vacancy-mediated diffusion in CrCoNi, we embed fifteen mono-vacancies randomly distributed in the system, followed by molecular dynamics simulations at 1,200 K. The choice of temperature allows a sufficient number of atomic jumps to occur at a simulation time of 2 ns. By tracking atomic migration, we obtain the displacement vectors at 2 ns, manifesting as net diffusion trajectories (Figs. 2a-b). It is of interest to see that, when comparing with RSS, the presence of SRO shortens the diffusion distance. We compute the MSD and aMSD for RSS and SRO as a function of time to quantify the effects of local chemical ordering. The MSD and aMSD data are presented in Fig. 2b, where the black colored circles are square displacements of RSS and brown colored ones for SRO. For RSS, the correlation factor $f = < \boldsymbol{R}^2 > / < \boldsymbol{R}^2{}_a > = 0.89$, and diffusivity is approximated to be $D_{\text{RSS}} = 0.0055$ Å^2/ns (i.e., 5.5×10^{-10}cm^2/s). The value of $f < 1$ indicates the non-random nature of diffusion in the RSS, that correlates diffusion jumps and reduces the effectiveness of atom jumps, thus $< \boldsymbol{R}^2 > < < \boldsymbol{R}^2{}_a >$. When SRO appears in the system, one can see the accumulated mean square displacement $< \boldsymbol{R}^2{}_a >$ is lowered as compared to that of RSS. The decrease of total square migration distance suggests that the SRO suppresses the atomic jump frequency by increasing the associated migration energy barrier. Notably, the MSD $< \boldsymbol{R}^2 >$ is further declined as a result of enhanced diffusion correlation (indicated by the correlation factor $f_{\text{SRO}} = 0.77$), which brings about a dif-

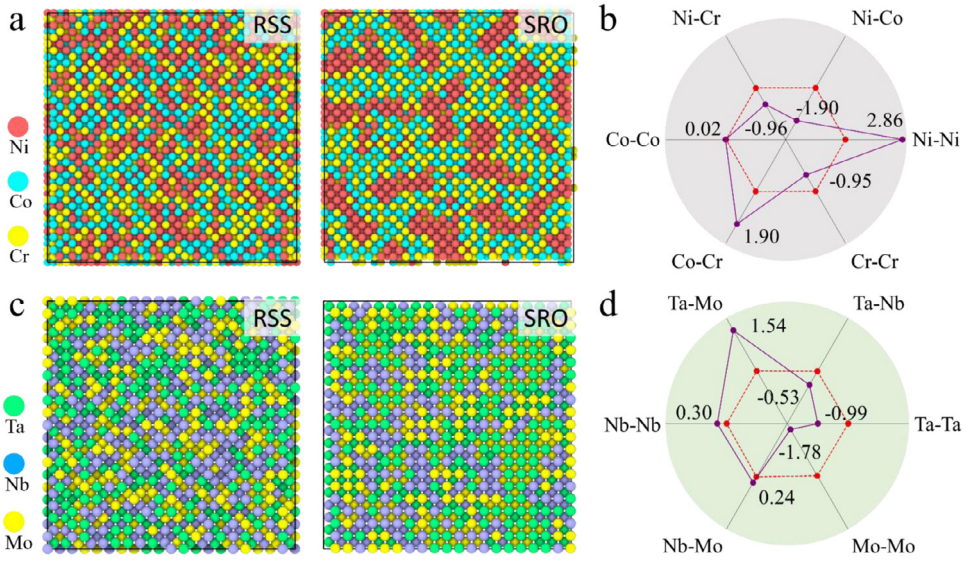

Fig. 1. Atomic configurations and their degree of ordering at first nearest neighbor in random solid solution (RSS) and system with short-range order (SRO). (a) CrCoNi configuration with RSS and SRO, and (b) shows the corresponding pairwise order parameters. (c-d) the same type of data for NbMoTa.

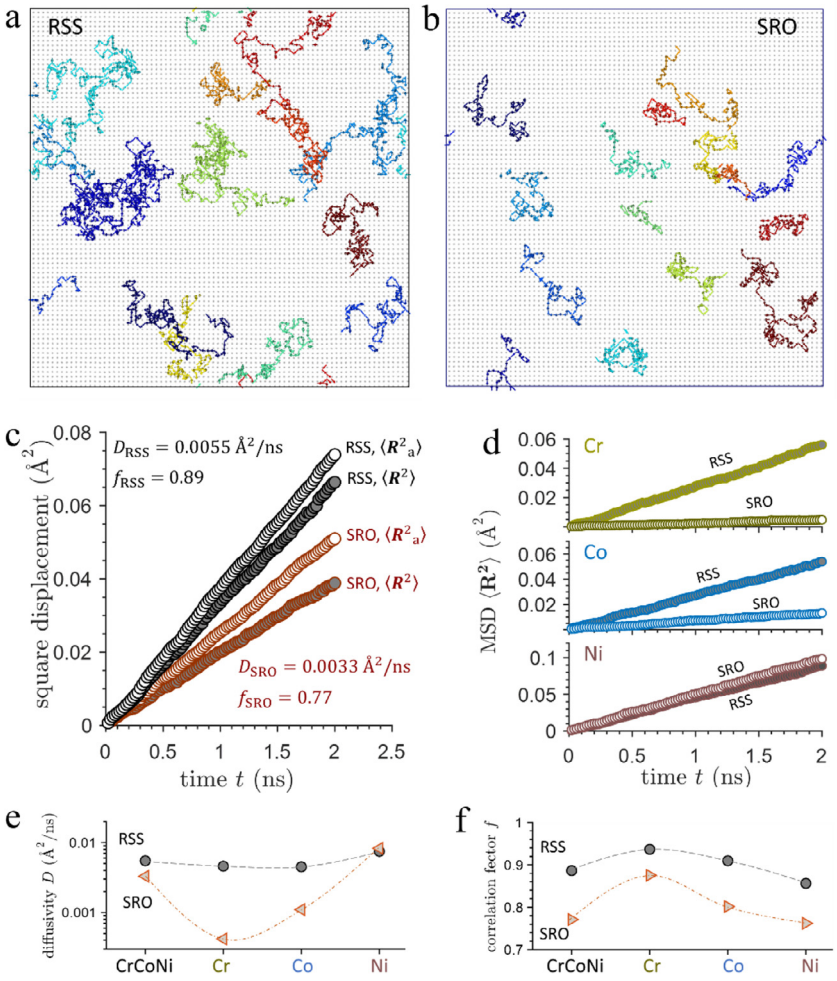

Fig. 2. Diffusion behavior in CrCoNi with RSS and SRO. (a-b) Diffusion trajectory at 1,200 K in RSS and SRO, respectively. (c) Mean square displacement $< \boldsymbol{R}^2 >$ and the accumulative square displacement $< \boldsymbol{R}^2_a >$ as a function of time t, and diffusivities and correlation factors are labeled. (d) Comparing elemental MSD in RSS and SRO. (e-f) show system-level and elemental diffusivities, and the diffusion correlation factors, respectively.

fusion coefficient D_{SRO} = 0.0033 Å^2/ns (i.e., 3.3×10^{10}cm^2/s) in the system with SRO. It is reasonable to assume that the presence of SRO considerably diminishes and localizes atomic diffusion, and this diffusion reduction originates from the decrease of atomic jump rate (implied by $< \boldsymbol{R}^2_a >$) and enhanced diffusion correlation (indicted by correlation factor f). In CoCrNi, SRO suppressing jump rate is the predominant factor responsible for diffusion-slowing down. In Fig. 2d, we present and compare the MSD of all constituent elements in RSS and SRO, as labeled. The diffusivities of Cr, Co markedly drop in magnitude with SRO (Fig. 2e), which account for the system-level diffusivity reduction, even if Ni diffusion rate remains essentially unchanged or slightly increases (see discussion of migration barrier regarding Fig. 4). It is worth noting that the correlation factors for all elements shift down to lower values in SRO, as shown in Fig. 2f. This implies the ordering in local chemistry weakens the degree of diffusion randomness and makes individual atomic jumps more correlated.

We move on to the discussion of refractory *bcc* NbMoTa, with the main results demonstrated in Fig. 3. It is evident by comparing the net migration trajectories in the two systems that the introduced SRO restrains atomic diffusion and shrinks the range of migration trajectory in this refractory system (Figs. 3a-b). Fig. 3c illustrates the variations of mean square displacement $< \boldsymbol{R}^2 >$ and the accumulative square displacement $< \boldsymbol{R}^2_a >$ with respect to time for RSS and SRO. The $< \boldsymbol{R}^2_a >$ of SRO is marginally smaller than that of RSS, implying that atoms in the two systems have comparable hopping frequency, and the introduced SRO does not drastically alter their underlying migration energy barrier. Considering the MSD $< \boldsymbol{R}^2 >$, the diffusivity of SRO (D_{SRO} = 0.0026 Å^2/ns) is significantly smaller than its RSS counterpart (D_{RSS} = 0.0035Å^2/ns), signifying the role of correlated diffusion on reducing the effectiveness of atomic jumps. Unlike SRO-induced diffusion reduction in CoCrNi, the enhanced diffusion correlation stemming from SRO is the dominating factor slowing down atomic diffusion of NbMoTa. To understand how individual elements respond to SRO, we show their MSDs and diffusivities in Figs. 3d-e, respectively. In the presence of SRO, the diffusion coefficients of all constituent components are lowered to various degrees, with Ta having the largest drop. Concerning correlation factor, the local chemical order renders the diffusion less random (seeing correlation factor f in Fig. 3f), and the more correlated diffusion can smear out some extent of atomic jumps, lowering the net square displacement (MSD or diffusivity).

In the potential energy landscape (PEL) perspective, vacancy-mediated atom diffusion appears as a saddle point hopping from an initial local energy minimum to an adjacent one. In single-component systems, all the migration pathways (jumps between nearest neighboring sites) and the associated migration barriers (jump frequency) are equivalent [19], implying a random walk nature. For MPEAs, however, the migration barriers and jump frequencies, depending on the local chemistry, can vary broadly, impacting diffusion randomness. When introducing SRO into MPEAs, the migration pathway and its underlying PEL can be additionally

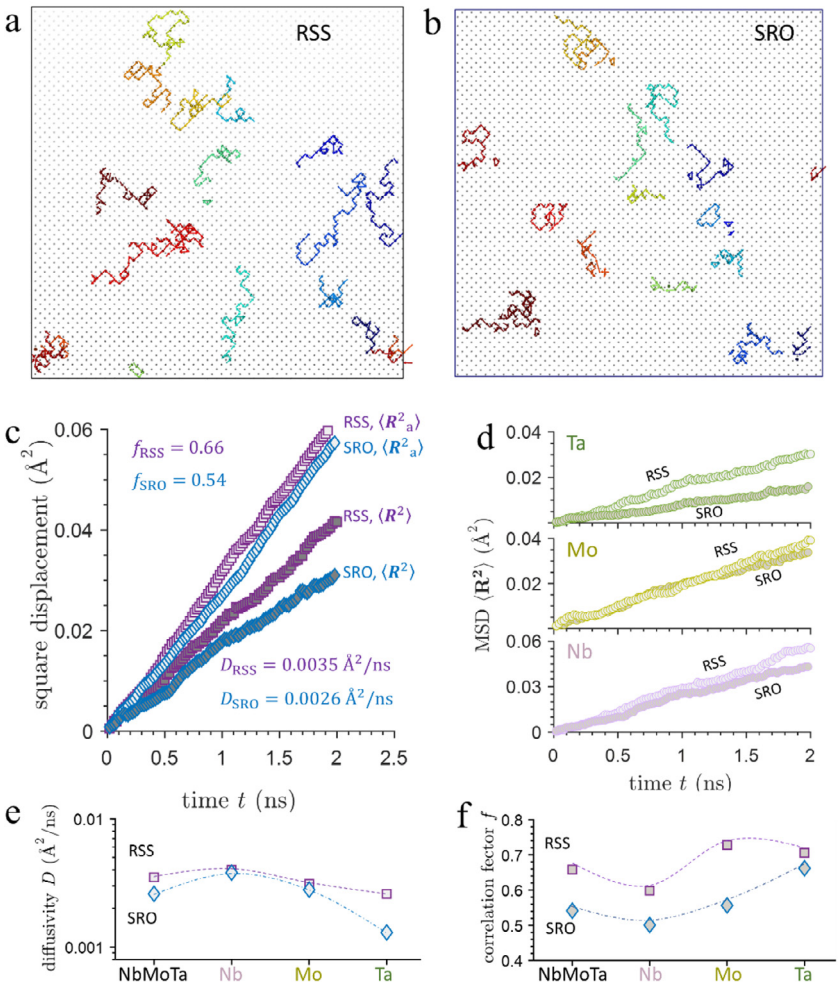

Fig. 3. Diffusion behavior in NbMoTa with RSS and SRO. (a-b) Diffusion trajectory at 2,000 K in RSS and SRO, respectively. (c) Mean square displacement $\langle \boldsymbol{R}^2 \rangle$ and the accumulative square displacement $\langle \boldsymbol{R}^2_a \rangle$ as a function of time t, and diffusivities and correlation factors are labeled. (d) Comparing elemental MSD in RSS and SRO. (e-f) show system-level and elemental diffusivities, and the diffusion correlation factors, respectively.

altered, which would influence atom jumps and hence diffusional behavior. To reveal the characteristics of the potential energy landscape governing diffusion, we sample and explore a significantly large number of atom-vacancy migration pathways and their associated energy barriers. For each alloy, we consider all possible migrations associated with 800 lattice sites; therefore, 9600 diffusion pathways are considered for *fcc* CrCoNi(12 jumps related to one site) and 6400 for *bcc* MoNbTa alloy (8 possible jumps per site). For each pathway, we compute the saddle point using climbing image nudged elastic band (NEB) method [20], from which the migration energy barrier is resolved.

The bottom panel of Fig. 4a exhibits the distributions of the migration energy barrier for RSS CrCoNi, and the distribution variance reflects the roughness of the potential energy landscape in which the diffusion jump takes place via saddle point hopping. With SRO, the barrier distribution spreads and becomes broader, implying the SRO stretches and roughens the PEL. Note that the overall migration barriers of Cr and Co shift towards a large value, suggesting an SRO-enhanced trapping effect. The *bcc* NbMoTa show a similar role of SRO on energy barrier widening, yet the mean values of migration barrier for Mo and Nb are insensitive to SRO (Fig. 4b). The increase in the migration barrier of Ta due to SRO is correlated with its diffusivity drop (see discussion of Figs. 3d-e).

As a vacancy migrates to a neighboring site, depending on its local chemical environments and the backward energy barrier, there is a likelihood that it can jump back to its original location. We compare the forward and backward migration barriers to sense the PEL feature, and their difference ($E_{\text{backward}} - E_{\text{forward}}$) is shown in Fig. 4c. The barrier differences in RSS materials follow a Gaussian distribution with the center position located at zero. That suggests, on average, the forward and backward jumps are equivalent. This is rational because the chemical surrounding migrating vacancies has the same extent of randomness. Interestingly, we note that barrier difference is skewed with SRO, and numerous negative values ($E_{\text{backward}} < E_{\text{forward}}$) appear, as shown in the bottom panel of Fig. 4c. The decrease of E_{backward} can come from the possible perturbation or interruption of local ordering due to element-vacancy switching that incurs an energy penalty on the final state. Because of the reduced backward barrier, the migrated atom would have an increased chance to jump back that cancels the effectiveness of the previous jump (enhancing diffusion correlation and decreasing MSD). Fig. 3d schematically depicts the influence of SRO on reshaping the PEL, in which the PEL structure is stretched and roughened by the SRO, manifesting as increased forward barrier and decreased backward barrier. The interplay between the trapping effect due to the enhanced forward barrier and jump correlation effect resulting from lowered backward barrier should directly impact diffusional behaviors, for instance, reducing and localizing diffusion.

Compared to dilute solid solutions, the MPEAs or HEAs exhibit extraordinary behaviors and properties, such as high creep resis-

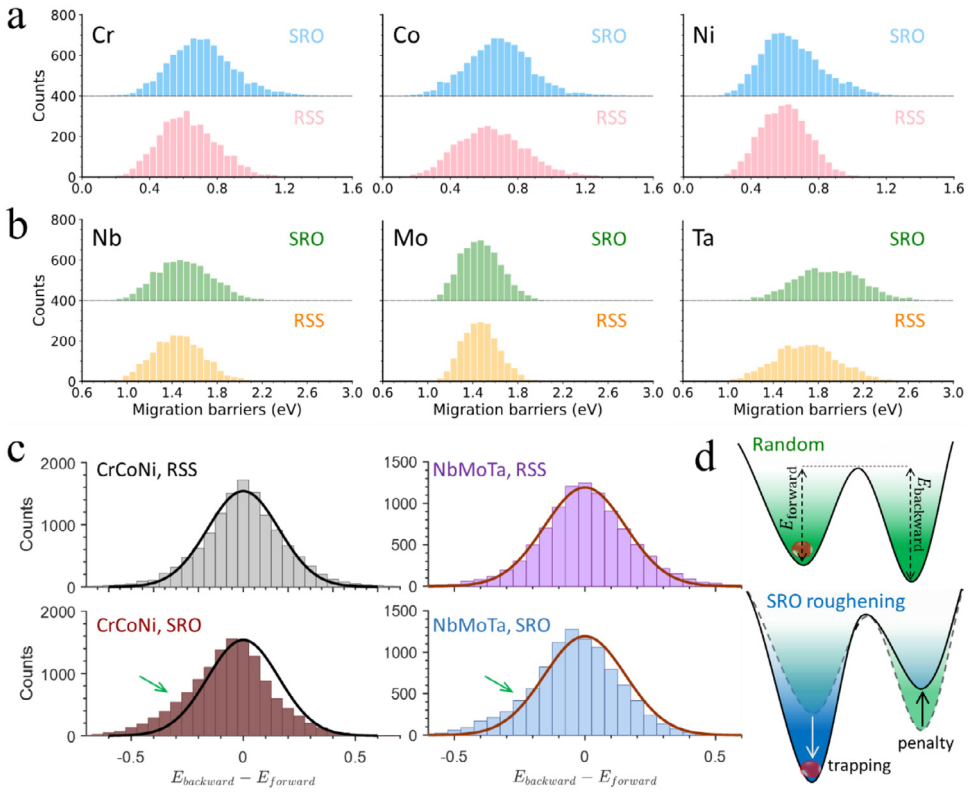

Fig. 4. (a-b) Distributions of the migration energy barrier for systems with SRO and RSS. (a) shows the results for CrCoNi and (b) for NaMoTa. (c) Backward and forward barrier difference ($E_{\text{backward}} - E_{\text{forward}}$) exhibits a Gaussian distribution in RSS, and SRO induces a shifting to the negative direction (i.e., $E_{\text{backward}} < E_{\text{forward}}$). (d) Schematic illustration of SRO effect on altering potential energy landscape structure, increasing forward barrier and reducing backward barrier.

tance and high thermal stability, closely related to their diffusion rates [8,16]. Because the actual MPEAs are processed, homogenized, or annealed at temperatures below their melting points, the SRO or local chemical ordering inevitably appears in the materials during these processes (due to mixing enthalpy and solute interactions) [21]. The nontrivial role of SRO on diffusion kinetics, revealed in this study, should be considered in future theoretical models and experimental measurements proposed to study diffusion-related behaviors of MPEAs [10]. This chemical ordering effect on diffusion is not exclusive to MPEAs and can be traced back to long-range ordered intermetallic. For example, the low diffusivity of B2 phase NiAl is speculated to result from the correlated jumps. The correlated jumps are induced by multiple possible mechanisms including six jump cycle [17], tripe defect and antistructural bridge [1]. These mechanisms contribute to preventing the disordering of B2 structures and each of them may take dominance over others under different temperatures and pressures. Our study, addressing the question about the role of SRO on the diffusion kinetics in MPEAs, found that increasing the degree of order can slow down diffusion rates. The diffusion reduction and localization originate from the stretched potential energy landscape by SRO that induces trapping effects and enhances diffusion correlation. The simulation results and theoretical analysis provide insight into fundamental diffusion processes in MPEAs, implying that tuning local chemical orders can serve as a strategy for manipulating diffusion-related properties.

Declaration of Competing Interest

The authors declare that they have no known competing financial interests or personal relationships that could have appeared to influence the work reported in this paper.

Acknowledgments

We gratefully acknowledge financial support from the U.S. Army Research Office under Grant No. W911NF-2110150. The authors acknowledge partial support from the National Science Foundation Materials Research Science and Engineering Center program through the UC Irvine Center for Complex and Active Materials (DMR-2011967).

References

[1] H. Mehrer, Springer Ser, Solid-State Sci (2007).
[2] J.-.W. Yeh, S.-.K. Chen, S.-.J. Lin, J.-.Y. Gan, T.-.S. Chin, T.-.T. Shun, C.-.H. Tsau, S.-.Y. Chang, Adv. Eng. Mater. 6 (2004) 299–303.
[3] B. Cantor, I.T.H. Chang, P. Knight, A.J.B. Vincent, Mater. Sci. Eng. A 375–377 (2004) 213–218.
[4] B. Schuh, F. Mendez-Martin, B. Völker, E.P. George, H. Clemens, R. Pippan, A. Hohenwarter, Acta Mater 96 (2015) 258–268.
[5] D.B. Miracle, O.N. Senkov, Acta Mater 122 (2017) 448–511.
[6] N.A.P.K. Kumar, C. Li, K.J. Leonard, H. Bei, S.J. Zinkle, Acta Mater 113 (2016) 230–244.
[7] H. Luo, Z. Li, A.M. Mingers, D. Raabe, Corros. Sci. 134 (2018) 131–139.
[8] E.P. George, D. Raabe, R.O. Ritchie, Nat. Rev. Mater. 4 (2019) 515–534.
[9] R. Zhang, S. Zhao, J. Ding, Y. Chong, T. Jia, C. Ophus, M. Asta, R.O. Ritchie, A.M. Minor, Nature 581 (2020) 283–287.
[10] P. Cao, Accounts Mater. Res. 2 (2021) 71–74.
[11] A. Einstein, Ann. Der Phys. 17 (1905) 549.
[12] M. von Smoluchowski, Ann. Phys. 326 (1906) 756–780.
[13] Q.-J. Li, H. Sheng, E. Ma, Nat. Commun. 10 (2019) 3563.
[14] X.-.G. Li, C. Chen, H. Zheng, Y. Zuo, S.P. Ong, Npj Comput. Mater. 6 (2020) 70.
[15] B. Sadigh, P. Erhart, A. Stukowski, A. Caro, E. Martinez, L. Zepeda-Ruiz, Phys. Rev. B 85 (2012) 184203.
[16] S. Nosé, Mol. Phys. 52 (1984) 255–268.
[17] W.G. Hoover, Phys. Rev. A 31 (1985) 1695–1697.
[18] J. Ding, Q. Yu, M. Asta, R.O. Ritchie, Proc. Natl. Acad, Sci 115 (2018) 8919–8924.
[19] M. Jin, P. Cao, M.P. Short, Acta Mater 147 (2018) 16–23.
[20] G. Henkelman, B.P. Uberuaga, H. Jónsson, J. Chem. Phys. 113 (2000) 9901–9904.
[21] Z. Shen, J.-.P. Du, S. Shinzato, Y. Sato, P. Yu, S. Ogata, Comput. Mater. Sci. 198 (2021) 110670.